Search for carbon-bearing compounds on low-albedo asteroids

T. Hromakina, M. A. Barucci, I. Belskaya, S. Fornasier, F. Merlin, A. Praet, G. Poggiali, M. Matsuoka

Monthly Notices of the ROYAL ASTRONOMICAL SOCIETY

MNRAS **514,** 21–33 (2022) https://doi.org/10.1093/mnras/stac1338
Advance Access publication 2022 May 13

Search for carbon-bearing compounds on low-albedo asteroids

T. Hromakina,[1,2]★ M. A. Barucci,[1] I. Belskaya,[2] S. Fornasier,[1,3] F. Merlin,[1] A. Praet,[1] G. Poggiali[1] and M. Matsuoka[1]

[1]*LESIA, Université Paris Cité, Observatoire de Paris, Université PSL, Sorbonne Université, CNRS, F-92190 Meudon, France*
[2]*V. N. Karazin Kharkiv National University, 4 Svobody Sq., Kharkiv, 61022, Ukraine*
[3]*Institut Universitaire de France (IUF), 1 rue Descartes, 75231 Paris Cedex 05, France*

Accepted 2022 May 6. Received 2022 May 6; in original form 2022 February 17

ABSTRACT

In this work, we aim to investigate the presence of absorption bands around 3.4 μm in the infrared spectra of primitive asteroids. We collected the published reflectance spectra of low-albedo asteroids from the literature and analysed the 2.4–3.8 μm region using the same techniques. From the initial data set of 92 asteroids, we restricted our analysis to 42 spectra of low-albedo asteroids with a good signal-to-noise (S/N) ratio, and we found the absorption feature around 3.4 μm in the spectra of 16 objects. For objects that are classified by the 3 μm band into the 'rounded', Ceres-like, and Europa-like groups, the depth of the 3.4 μm feature is strongly correlated with that of the 3 μm band. The majority of objects in our data set not showing the 3.4 μm absorption band have lower S/N spectra and belong to Ch or Chg classes, while asteroids with a detected 3.4 μm bands mostly belong to C, B, and also P types. Additionally, asteroids with a detected 3.4 μm band tend to have a lower albedo, redder J-K colours, and more neutral U-V colours. We observe that the analysed objects larger than ∼300 km in diameter show features due to carbon-bearing materials, which could be explained by their higher S/N ratio in our data set. Finally, we found that the distributions of asteroids showing the 3.4 μm feature appear to be shifted towards larger distances from the Sun compared to those not showing this band.

Key words: techniques: spectroscopic – minor planets, asteroids: general.

1 INTRODUCTION

The study of carbon-bearing materials, which could be associated with carbonates and organics, in small Solar System objects and meteorites provides us with knowledge about the processes that took place at the early stages of Solar System formation and may give some insights into the origin of life on Earth. Organic materials are widely present in various groups of carbonaceous chondrites (Hayes 1967; Robert & Epstein 1982; Botta & Bada 2002; Alexander et al. 2007) believed to have originated from dark primitive asteroids (Bell 1989; Gaffey, Burbine & Binzel 1993; Pieters & McFadden 1994), but rarely detected on the latter.

One of the effective methods to detect organic matters remotely is near-infrared spectroscopic observations (Keller et al. 2004; Kebukawa et al. 2010b; Kebukawa, Nakashima & Zolensky 2010a). In particular, the region between 2.8 and 3.6 μm is affected by the presence of features related to several functional groups such as carbon-hydrogen (C-H), oxygen-hydrogen (O-H), and nitrogen-hydrogen (N-H) (Raponi et al. 2020). Unambiguous detection of organic materials using near-infrared spectroscopy is very difficult due to an overlap between organic and carbonate (CO_3^{2-}-bearing minerals) features in the 3.2–3.6 μm spectral region (Alexander et al. 2014; Nuevo et al. 2014). For organic compounds, the absorption bands at 3.38 and 3.42 μm are assigned to asymmetric C-H stretching modes of methyl (CH_3) and methylene (CH_2) aliphatic groups, respectively (Moroz et al. 1998). Moreover, an absorption band at 3.47 μm is assigned to the aliphatic C-H stretching symmetric modes of CH_3 and CH_2 groups. The absorption feature at 3.3 μm could be attributed to polycyclic aromatic hydrocarbons (PAHs), and the absorption bands around 3.1 and 3.3 μm could also be related to N-H vibrations (Raponi et al. 2020). These features are observed in both synthetic and natural carbonaceous material, as well as in meteoritic spectra (Mennella 2010; Kaplan et al. 2019).

Infrared laboratory measurements have been performed for various classes of carbonaceous chondrites, such as CI, CM, CV, CK, CR, and C2 ungrouped (see Takir et al. 2019, and references therein). These meteorites are associated with the C- and D-complex asteroids, which are among the darkest asteroids in the Solar System. Some meteorite infrared measurements focused on the search for organics were performed in the past.

Features around 3.4–3.5 μm were observed both in transmission/absorbance (Orthous-Daunay et al. 2013; Ehrenfreund et al. 1991) and reflectance (Takir et al. 2013; Beck et al. 2018; Kaplan et al. 2019) although in the latter case the features are fainter and in any case for many sample ambiguity remains as to whether the samples may be contaminated from Earth organics. Beck et al. (2018) suggests that the strength of this absorption feature is determined by both carbon abundance and the H/C ratio of the organics.

The majority of organic material in carbonaceous chondrites is attributed to insoluble organic matter (IOM), a kerogen-like macromolecular material (Pizzarello, Cooper & Flynn 2006;

★ E-mail: tetiana.hromakina@obspm.fr

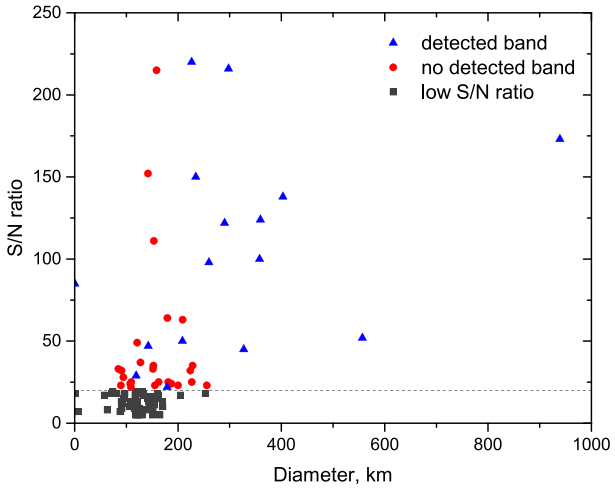

Figure 1. Diameter versus S/N ratio in the 3.3–3.5 μm wavelength range for asteroids in our data set. In the case when multiple spectra are available for an object, the one with the higher S/N ratio is considered.

Schmitt-Kopplin et al. 2010). IOM in meteorites is believed to have originated from the interstellar medium (ISM), but an origin in the outer Solar System is not completely ruled out (Busemann et al. 2006; Alexander et al. 2017). Cody & Alexander (2005) found a wide range in the composition of IOM for primitive chondrites. The authors suggest that such variation is related to a low-temperature chemical oxidation of the aliphatic fraction. There is also a certain link between the IOM in meteorites and the interplanetary dust particles that are the fragments of asteroids and comets (Keller et al. 2004; Busemann et al. 2006). In particular, the chemical composition of IOM in meteorites is similar to that of CHON grains of comet Halley (Fomenkova, Chang & Mukhin 1994; Nakamura-Messenger et al. 2006; Alexander et al. 2007).

The first tentative identification of an absorption band at 3.4 μm was made for asteroid (130) Elektra (Cruikshank & Brown 1987). The presence of this feature in the spectrum of Elektra was not confirmed by the later surveys of dark asteroids (Jones et al. 1990; Cruikshank et al. 2002). However, the quality of the spectra was too low to identify a feature with a depth of less than $\sim$ 7% (Cruikshank et al. 2002). Absorption features centred around 3.3–3.5 μm were also found for asteroids (24) Themis (Campins et al. 2010; Rivkin & Emery 2010) and (65) Cybele (Licandro et al. 2011), for the irregular Jupiter satellite Himalia (Brown & Rhoden 2014), and for Saturn's moons Phoebe (Cruikshank et al. 2014), Iapetus (Cruikshank et al. 2014), and Hyperion (Brad Dalton, Cruikshank & Clark 2012). A potential weaker absorption around 3.3–3.5 μm was detected in the mean spectra of Jupiter Trojans characterized by a less steep spectral slope (Brown 2016).

New results on the identification of carbon-bearing compounds were obtained thanks to *in situ* spectral observations of primordial small Solar System objects. These observations include comet 67P/Churyumov-Gerasimenko observed by the Rosetta space mission (Capaccioni et al. 2015), the dwarf planet (1) Ceres studied by the Dawn space mission (De Sanctis et al. 2019, 2017), and two near-Earth asteroids (101955) Bennu and (162173) Ryugu, visited by the OSIRIS-REx (Lauretta et al. 2019) and Hayabusa2 (Watanabe et al. 2017) space missions, respectively. In the spectra of comet 67P/Churyumov-Gerasimenko, the absorption bands at 3.38 and 3.42 μm have been assigned to asymmetric C-H stretching modes of the methyl (CH_3) and methylene (CH_2) aliphatic groups, respectively, while the one at 3.47 μm is attributed to the symmetric modes of CH_3 and CH_2 groups (Raponi et al. 2020). For (1) Ceres, the absorption features between 3.3 and 3.6 μm have been attributed to overlapping absorptions of carbonates and organic matter (De Sanctis et al. 2019, 2017). The presence of an absorption feature at 3.4 μm was also detected for asteroid (101955) Bennu (Kaplan et al. 2020). The C-type asteroid Ryugu shares some physical properties with Bennu. Although direct detection of organics on Ryugu's surface was not possible due to the limit in the spectroscopic range observed by spacecraft instruments, initial analysis of samples returned to Earth revealed the presence of an absorption feature at 3.4 μm linked to the presence of organics on a global scale. As well as the presence of carbonate grains distinguishable by the double peak at 3.32 and 3.455 μm (Pilorget et al. 2021; Yada et al. 2021).

In this work, we aimed to investigate organic material in primordial low-albedo asteroids. We thus looked for available spectra covering the 3–3.6 μm region, and by implementing the same techniques for all the collected data, we carried out a homogeneous analysis to identify and to characterize the feature around 3.3–3.5 μm, when present. We also looked for possible correlations between the presence of the absorption band and the physical and orbital properties of asteroids.

2 METHODS

We collected all the available infrared spectral data for low-albedo asteroids belonging to the C-complex (including B-type) and D-type, following the DeMeo et al. (2009) classification scheme, and the P-type asteroids from the Tholen taxonomy (Tholen 1984, the P-type are part of the X-complex in the DeMeo taxonomy). In total, the initial data set included 92 asteroids (see Table A in the Appendix). For some of the objects multiple spectra are available, which bring a total of 122 individual spectra covering the 3–4 μm range.

The spectra from Lebofsky et al. (1981), Feierberg, Lebofsky & Tholen (1985), and Jones et al. (1990) were taken from the PDS Small Bodies Node database,[1] the spectra from Usui et al. (2019) were taken from the AKARI database,[2] and the rest of the spectra were digitized using the WEBPLOTDIGITIZER software (Rohatgi 2021). All the collected spectra were originally thermally corrected by the authors in the respective works. We note that the collected spectra were acquired using several instruments and at different observational conditions, thus the resulting data set is quite heterogeneous.

For the analysis, we selected the spectra with resolution high enough to search for absorption features around 3.4 μm. The selection was based on the signal-to-noise (S/N) ratio criterion. The S/N was computed for spectra that were normalized at 2.4 μm as the inverse value of the mean error in the 3.2–3.6 μm range. For spectra taken from databases, we used the reported uncertainties. To acquire the uncertainties of the digitized data, which were not directly collected by the digitalization procedure, the spectra were binned. The bin size was optimized for each spectrum with bins typically contained 3–5 data points. As a result, the bin step ranges from 0.01 to 0.03 μm. Then, assuming that the neighbouring points

[1] https://pds.nasa.gov/ds-view/pds/viewProfile.jsp?dsid=EAR-A-3-RDR-THREEMICRON-V1.1
[2] https://www.ir.isas.jaxa.jp/AKARI/Archive/

Table 1. List of primitive asteroids selected for the analysis on the basis of S/N ratio.

	Object	Taxon	p_v	D, km	J-K	U-V	SNR	3.4 μm band	Spectrum reference
1	(1) Ceres	C	0.064 ± 0.013	939.4 ± 0.20	0.46 ± 0.03	1.14 ± 0.03	173	Yes	Rivkin, Volquardsen & Clark (2006)
2	(2) Pallas	B	0.117 ± 0.023	556.99 ± 55.70	0.32 ± 0.03	0.92 ± 0.04	52	Yes	Usui et al. (2019)
3	(10) Hygiea	C	0.069 ± 0.014	402.96 ± 40.30	0.47 ± 0.03	1.05 ± 0.04	138	Yes	Rivkin, Howell & Emery (2019)
4	(13) Egeria	Ch	0.078 ± 0.016	208.92 ± 20.89	0.40 ± 0.03	1.20 ± 0.04	34	No	Usui et al. (2019)
5	(19) Fortuna	Ch	0.045 ± 0.011	224.13 ± 22.41		1.04 ± 0.05	32	No	Rivkin et al. (2015)
6	(24) Themis	B	0.055 ± 0.011	208.73 ± 20.87	0.53 ± 0.03	1.02 ± 0.04	50	Yes	Rivkin & Emery (2010)
7	(31) Euphrosyne	Cb	0.041 ± 0.008	289.99 ± 29.00	0.57 ± 0.03	1.00 ± 0.03	122	Yes	Rivkin et al. (2019)
8	(41) Daphne	Ch	0.064 ± 0.013	179.71 ± 17.97	0.42 ± 0.03	1.09 ± 0.02	64	No	Rivkin et al. (2015)
9	(48) Doris	Ch	0.053 ± 0.011	228.47 ± 22.85	0.36 ± 0.03	1.16 ± 0.02	35	No	Takir & Emery (2012)
10	(49) Pales	Ch	0.057 ± 0.023	155.18 ± 31.04		1.16 ± 0.06	23	No	Usui et al. (2019)
11	(50) Virginia	Ch	0.047 ± 0.009	89.53 ± 8.95	0.42 ± 0.03	1.05 ± 0.05	23	No	Usui et al. (2019)
12	(51) Nemausa	Cgh	0.069 ± 0.014	158.59 ± 15.86		1.27 ± 0.02	215	No	Rivkin et al. (2015)
13	(52) Europa	C	0.040 ± 0.008	359.53 ± 35.95		1.02 ± 0.03	124	Yes	Takir & Emery (2012)
14	(54) Alexandra	Cgh	0.061 ± 0.012	152.48 ± 15.25	0.37 ± 0.02	1.08 ± 0.05	35	No	Takir & Emery (2012)
15	(56) Melete	X, P	0.062 ± 0.012	109.00 ± 10.90	0.51 ± 0.03	1.01 ± 0.05	22	No	Usui et al. (2019)
16	(65) Cybele	X, P	0.038 ± 0.008	297.85 ± 20.79	0.56 ± 0.03	0.96 ± 0.03	216	Yes	Licandro et al. (2011)
17	(70) Panopaea	Cgh	0.053 ± 0.011	142.1 ± 14.21	0.42 ± 0.02	1.13 ± 0.03	152	No	Rivkin et al. (2015)
18	(78) Diana	Ch	0.060 ± 0.012	121.14 ± 12.11	0.44 ± 0.02	1.09 ± 0.03	49	No	Rivkin et al. (2015)
19	(88) Thisbe	B	0.047 ± 0.009	226.21 ± 22.62	0.50 ± 0.03	0.99 ± 0.02	220	Yes	Rivkin et al. (2019)
20	(91) Aegina	Ch	0.045 ± 0.009	107.86 ± 10.79	0.34 ± 0.03	1.04 ± 0.04	24	No	Takir & Emery (2012)
21	(105) Artemis	Ch	0.037 ± 0.011	127.41 ± 12.74		1.01 ± 0.03	37	No	Rivkin et al. (2015)
22	(106) Dione	Cgh	0.063 ± 0.011	162.62 ± 16.26		1.21 ± 0.03	25	No	Usui et al. (2019)
23	(107) Camilla	X, P	0.063 ± 0.013	199.96 ± 20.00	0.56 ± 0.03	1.00 ± 0.03	23	No	Takir & Emery (2012)
24	(109) Felicitas	Ch	0.066 ± 0.010	84.58 ± 16.92		1.10 ± 0.02	33	No	Rivkin et al. (2015)
25	(121) Hermione	Ch	0.043 ± 0.009	226.6 ± 22.66		1.16 ± 0.09	63	No	Usui et al. (2019)
26	(130) Elektra	Ch	0.077 ± 0.010	181.18 ± 18.12	0.51 ± 0.02	1.24 ± 0.04	25	No	Takir & Emery (2012)
27	(140) Siwa	X, P	0.068 ± 0.015	109.88 ± 10.99	0.54 ± 0.03	1.02 ± 0.04	20	No	Takir & Emery (2012)
28	(144) Vibilia	Ch	0.048 ± 0.010	151.56 ± 15.16	0.47 ± 0.02	1.13 ± 0.05	33	No	Rivkin et al. (2015)
29	(190) Ismene	X, P	0.049 ± 0.020	187.08 ± 37.42	0.63 ± 0.03	0.95 ± 0.03	24	No	Takir & Emery (2012)
30	(308) Polyxo	T	0.052 ± 0.010	142.41 ± 14.24	0.48 ± 0.04	1.16 ± 0.03	47	Yes	Takir & Emery (2012)
31	(324) Bamberga	Cb	0.051 ± 0.010	234.36 ± 23.44		1.00 ± 0.04	150	Yes	Rivkin et al. (2019)
32	(334) Chicago	C	0.052 ± 0.010	179.17 ± 17.92	0.47 ± 0.04	1.09 ± 0.04	22	Yes	Takir & Emery (2012)
33	(361) Bononia	D	00.037 ± 0.007	153.15 ± 15.32	0.67 ± 0.04	1.01 ± 0.03	111	No	Takir & Emery (2012)
34	(404) Arsinoe	Ch	0.047 ± 0.009	94.39 ± 9.44	0.39 ± 0.05	1.01 ± 0.04	28	No	Rivkin et al. (2015)
35	(407) Arachne	Ch	0.056 ± 0.011	90.85 ± 9.08	0.36 ± 0.02	1.07 ± 0.04	32	No	Rivkin et al. (2015)
36	(423) Diotima	C	0.034 ± 0.007	255.82 ± 25.58		0.98 ± 0.02	23	No	Usui et al. (2019)
37	(451) Patientia	Cb	0.056 ± 0.011	259.74 ± 25.97	0.51 ± 0.03	0.98 ± 0.05	98	Yes	Rivkin et al. (2019)
38	(476) Hedwig	X, P	0.049 ± 0.010	118.93 ± 11.89	0.51 ± 0.02	1.09 ± 0.04	29	No	Usui et al. (2019)
39	(511) Davida	C	0.047 ± 0.009	327.34 ± 32.73	0.51 ± 0.02	1.08 ± 0.02	45	Yes	Takir & Emery (2012)
40	(704) Interamnia	B	0.044 ± 0.009	358.13 ± 35.81	0.50 ± 0.02	0.90 ± 0.03	100	Yes	Rivkin et al. (2019)
41	(101955) Bennu	B	0.044 ± 0.002	0.490 ± 0.001			85	Yes	Merlin et al. (2021)
42	(162173) Ryugu	C	0.040 ± 0.005	0.865 ± 0.015			>1000	Yes	Yada et al. (2021)

Taxonomic types follow the classification by DeMeo et al. (2009). For some objects, we provide classification following the definitions by both DeMeo et al. (2009) and Tholen (1984), as the later takes into account the albedo value of the object and thus is more precise.
Geometric albedos (p_v) and diameters (D) are taken from AKARI IRC asteroid flux catalogue (Alí-Lagoa et al. 2018), except the diameter and albedo of (1) Ceres and (101955) Bennu, which were taken from Park et al. (2016) and Lauretta et al. (2019), respectively. For (162173), Ryugu albedo value was taken from Tatsumi et al. (2020) and diameter is from Müller et al. (2017).
J-K and U-V colours are from Sykes et al. (2010) and Tedesco (2005), respectively.

have similar uncertainties, the errors were derived as the standard deviation of data points in each bin. We found that for all the spectra of studied asteroids the estimated original errors are comparable with those derived through data binning.

We decided to keep in the data set the spectra having S/N ratio > 20, i.e. permitting to identify potential absorption features at 3.4 μm deeper than 5 per cent (Fig. 1). A complete list of low-albedo asteroids with the corresponding S/N ratio and reference to the best quality spectra is presented in Table A of the Appendix. Applying this criterion, the data set of low albedo asteroids that we finally investigated was restricted to 42 objects. Table 1 shows the list of the final 42 objects alongside with their respective diameters as well as J-K and U-V colours (Tedesco 2005; Sykes et al. 2010).

To characterize the absorption bands in the 3 μm region, we first removed the spectral continuum computed by a simple linear fit that was evaluated at the edges of the features. The anchor points were fixed in the areas around 2.35–2.45 and 3.75-3–85 μm (except for (2) Pallas with anchor points around 2.55–2.65 and 3.60–3.70 μm due to spectrum cut-off), thus the whole broad 3 μm feature was included into our analysis. The region in the 2.4–3.8 μm wavelength range was fitted by multiple Gaussian profiles. Gaussian functions were previously used to describe the absorption feature due to

Table 2. Characteristics of the 3 and 3.4 μm bands in the spectra of low-albedo asteroids asteroids obtained using ground-based and space telescopes.

	Object	3 μm band centre, μm	3.4 μm band centre, μm	3 μm band per cent	3.4 μm band depth, per cent	3 μm type∗	Spectrum reference
1	(1) Ceres	3.006 ± 0.001	3.414 ± 0.001	20.30 ± 0.03	8.83 ± 0.06	Ceres-type	Rivkin et al. (2011)
		3.027 ± 0.005	3.390 ± 0.006	17.12 ± 0.13	9.23 ± 0.28		Rivkin et al. (2019)
2	(2) Pallas	2.748 ± 0.042	3.283 ± 0.104	33.7 ± 0.70	4.53 ± 0.81	Sharp	Usui et al. (2019)
3	(10) Hygiea	3.055 ± 0.001	3.398 ± 0.001	7.88 ± 0.02	3.41 ± 0.03	Ceres-type	Rivkin et al. (2011)
		3.054 ± 0.025	3.396 ± 0.056	5.61 ± 0.46	2.33 ± 1.74		Rivkin et al. (2019)
		2.973 ± 0.039	3.348 ± 0.052	8.06 ± 1.13	6.54 ± 0.74		Rivkin et al. (2019)
		3.048 ± 0.006	3.414 ± 0.011	11.52 ± 0.25	4.99 ± 0.48		Rivkin et al. (2019)
		3.000 ± 0.008	3.414 ± 0.013	11.77 ± 0.20	4.86 ± 0.32		Rivkin et al. (2019)
		2.892 ± 0.026	3.366 ± 0.048	16.97 ± 0.66	8.18 ± 3.06		Takir & Emery (2012)
		2.745 ± 0.014	3.452 ± 0.050	16.70 ± 0.63	3.57 ± 0.77		Usui et al. (2019)
4	(24) Themis	3.092 ± 0.000	3.420 ± 0.001	11.93 ± 0.49	5.67 ± 0.23	Round	Rivkin & Emery (2010)
		3.078 ± 0.004	3.400 ± 0.054	14.03 ± 1.28	5.85 ± 1.18		Campins et al. (2010)
5	(31) Euphrosyne	3.088 ± 0.020	3.396 ± 0.063	7.52 ± 0.71	2.70 ± 1.59	Europa-type	Rivkin et al. (2019)
		3.098 ± 0.025	3.387 ± 0.238	4.73 ± 0.72	2.31 ± 0.94		Rivkin et al. (2019)
		3.092 ± 0.013	3.447 ± 0.069	5.69 ± 0.49	1.60 ± 0.47		Rivkin et al. (2019)
		3.066 ± 0.017	3.403 ± 0.040	7.71 ± 0.57	2.49 ± 0.59		Rivkin et al. (2019)
		3.035 ± 0.015	3.394 ± 0.164	9.68 ± 1.49	3.61 ± 0.73		Takir & Emery (2012)
6	(52) Europa	3.073 ± 0.021	3.401 ± 0.068	8.55 ± 0.45	3.64 ± 0.74	Europa-type	Rivkin et al. (2019)
		3.009 ± 0.012	3.349 ± 0.017	11.30 ± 0.27	4.31 ± 0.73		Takir & Emery (2012)
7	(65) Cybele	3.049 ± 0.083	3.329 ± 0.053	9.62 ± 1.36	4.05 ± 0.64	Rounded	Hargrove et al. (2012)
		2.857 ± 0.005	3.369 ± 0.001	9.19 ± 1.40	3.88 ± 1.27		Licandro et al. (2011)
8	(88) Thisbe	3.060 ± 0.014	3.399 ± 0.062	7.04 ± 0.65	2.09 ± 0.31	Rounded	Rivkin et al. (2019)
		3.014 ± 0.076	3.367 ± 0.185	8.32 ± 1.70	4.93 ± 1.11		Rivkin et al. (2019)
9	(308) Polyxo	—	—	21.21 ± 4.82	8.28 ± 1.59	Sharp	Takir & Emery (2012)
10	(324) Bamberga	3.011 ± 0.018	3.443 ± 0.042	4.17 ± 0.32	1.63 ± 0.26	Ceres-type	Rivkin et al. (2019)
		3.023 ± 0.009	3.469 ± 0.015	6.80 ± 0.15	2.65 ± 0.29		Rivkin et al. (2019)
11	(334) Chicago	—	—	10.70 ± 2.42	8.66 ± 3.76	Sharp	Takir & Emery (2012)
12	(451) Patientia	3.042 ± 0.015	3.402 ± 0.055	9.19 ± 0.37	3.06 ± 0.86	Europa-type	Rivkin et al. (2019)
		2.979 ± 0.023	3.406 ± 0.173	12.23 ± 2.24	6.06 ± 0.05		Takir & Emery (2012)
13	(511) Davida	—	—	12.41 ± 1.99	6.52 ± 1.26	Sharp	Takir & Emery (2012)
		2.747 ± 0.008	3.371 ± 0.182	24.35 ± 1.58	4.29 ± 1.57		Usui et al. (2019)
14	(704) Interamnia	—	—	7.77 ± 0.53	3.08 ± 0.46	Sharp	Rivkin et al. (2019)
		2.922 ± 0.055	3.407 ± 0.097	5.74 ± 0.56	2.84 ± 0.53		Rivkin et al. (2019)

∗Following the classification by Takir & Emery (2012).

hydrated phyllosilicates in the spectra of asteroids and meteorites. As the 3 μm feature consists of several OH stretching modes, up to five Gaussians were used to model this spectral range (see Kaplan et al. (2019) and Praet et al. (2021) for details on the method). As this method is associated with a large number of free parameters, we do not seek to distinguish all the components of the broad 3 μm feature, but used the minimal number of curves required to fit our area of interest. Thus, depending on the shape of the 3 μm feature and on the S/N of the spectra, a total of two or three Gaussian functions were used. The band around 3.4 μm was always fitted using one Gaussian function, whereas the larger 3 μm band was fitted with one (in most of the cases) or two Gaussian functions (in the case of (1) Ceres, (2) Pallas, (24) Themis, (65) Cybele, and (101955) Bennu) to achieve a good fit. The centre and the amplitude of the fitted Gaussian curves were used to determine the position and depth of the absorption bands. For (1) Ceres, (2) Pallas, and (101955) Bennu, the position and depth of the 3 μm band were calculated at the minimum of the multiple Gaussian fit. Errors were computed using a Monte Carlo method by randomly sampling data 100 times and taking the standard deviation as uncertainty.

3 RESULTS

Applying the method presented above to our data set of 42 objects we identified the 3.4 μm feature in the spectra of 16 asteroids. A list of asteroids with spectra showing a 3.4 μm feature and the derived band parameters for both 3 and 3.4 μm bands are reported in Table 2. In spectra of asteroids (308) Polyxo, (334) Chicago, (511) Davida, and (704) Interamnia data around 3 μm are partially missing, so we do not present the 3 μm band parameters for these objects. We also note that the spectral resolution of the original data and consequently the binned spectra in our data set is not sufficient to distinguish if the 3.4 μm band is associated with carbonate-dominated or organic-dominated materials.

The 16 asteroids having an absorption band around 3.4 μm also show absorption features in the 2.7–3.1 μm region attributed to hydrated minerals, water ice, or NH bearing compounds. We thus grouped the 16 asteroids showing the 3.4 μm features into four groups following the Takir & Emery (2012) classification scheme, i.e. 'sharp', Ceres-type, Europa-type, and 'rounded'. The objects classified into the 'sharp' group include (2) Pallas, (308) Polyxo, (334) Chicago, (511) Davida, (704) Interamnia, (101955) Bennu, and (162173) Ryugu. Their spectra are shown in Fig. 2, except for (101955) Bennu and (162173) Ryugu that are shown and discussed separately. Ceres-type spectra include (1) Ceres, (10) Hygiea, and (324) Bamberga and are presented in Fig. 3. Finally, Europa-type spectra include (31) Euphrosyne, (52) Europa, and (451) Patientia that are shown in Fig. 4. 'Rounded' group consists of (24) Themis, (65) Cybele, and (88) Thisbe (Fig. 5).

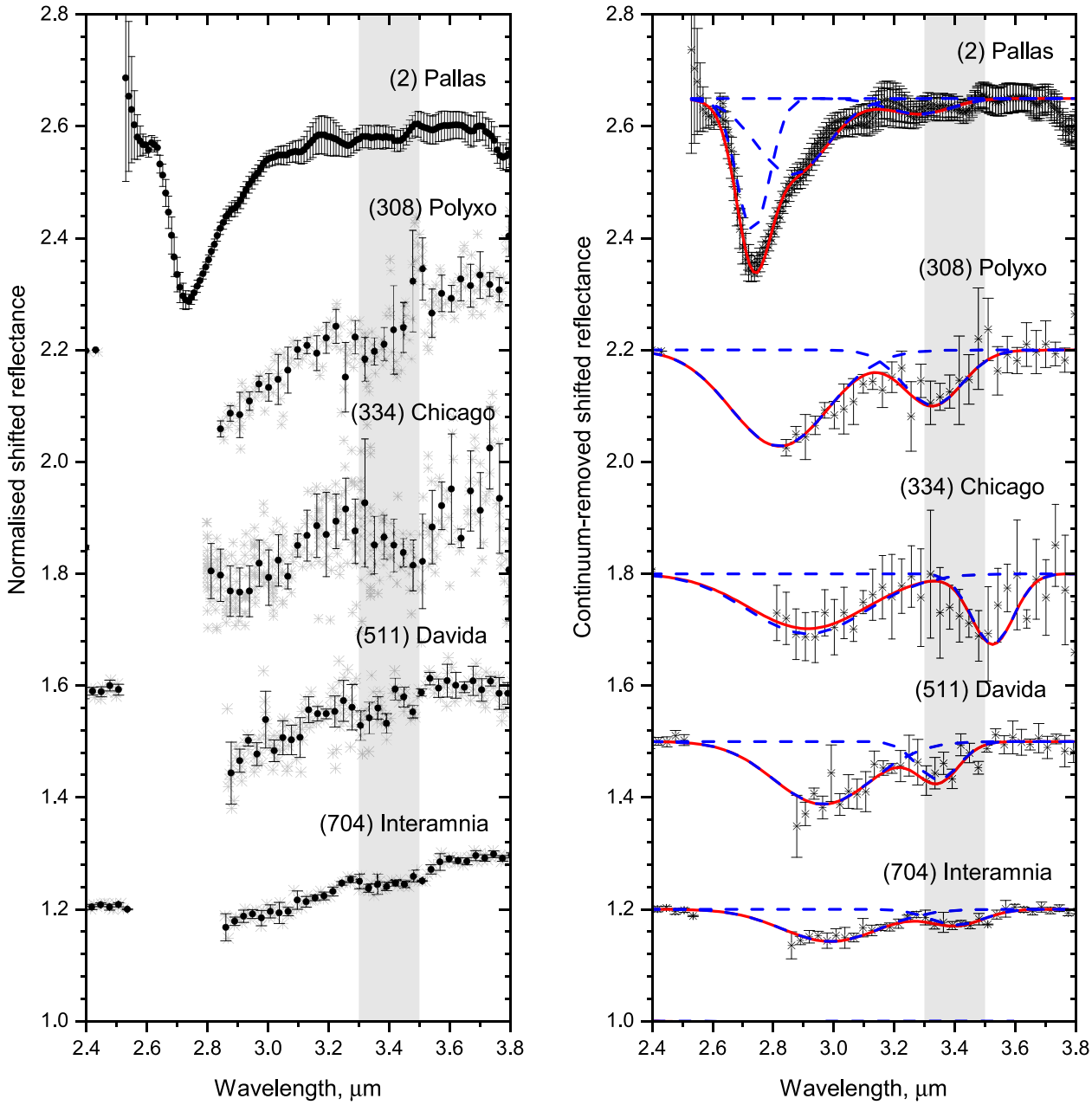

Figure 2. Primitive asteroids of the 'sharp' group following Takir & Emery (2012) classification showing both the 2.7 and 3.4 μm features. The spectrum of (2) Pallas is from Usui et al. (2019); (308) Polyxo, (334) Chicago, and (511) Davida are from Takir & Emery (2012); and the spectrum of (704) Interamnia is from Rivkin et al. (2019). The spectra are shifted for clarity. The left-hand panel shows the spectra normalized at 2.4 μm (except the spectra of (2) Pallas which was normalized at 2.55 μm). The original digitized spectra for which the binning was applied are shown in grey. The right-hand panel shows continuum-removed spectra together with the fit of the overall spectrum using multiple Gaussian functions (solid red line) and the individual Gaussian functions used to fit each spectrum (dashed blue line). The 3.3–3.5 μm grey area highlights the 3.4 μm absorption band.

Comet 67P is also classified into this group and we show its high-resolution spectra, acquired *in situ* by the Rosetta mission (Raponi et al. 2020), for comparison.

Following the taxonomic classification by DeMeo et al. (2009), the majority of objects in this work belong to the C-complex group. The rest of the objects belong to X-group (or P-type following the classification by Tholen (1984), D-, and T-type). Notably, a total of 19 aqueously altered Ch and Cgh type asteroids in our data set do not show the 3.4 μm band. This asteroid class is defined by having an absorption band near 0.7 μm associated with phyllosilicates (accompanied by the 2.7–3 μm feature). However, only two Ch/Chg asteroids in the data set ((51) Nemausa and (78) Diana) have high S/N spectra. Thus, the fact that the 3.4 μm band is not detected for Ch and Cgh type asteroids can be related to the generally lower S/N ratio and thus to a shallower 3.4 μm band for these groups.

3.1 Results for space mission targets

Among all the asteroids showing a 3.4 μm band in our data set only three (Ceres, Bennu, and Ryugu) were targets of the space missions. For (1) Ceres and (101955) Bennu global spectra that

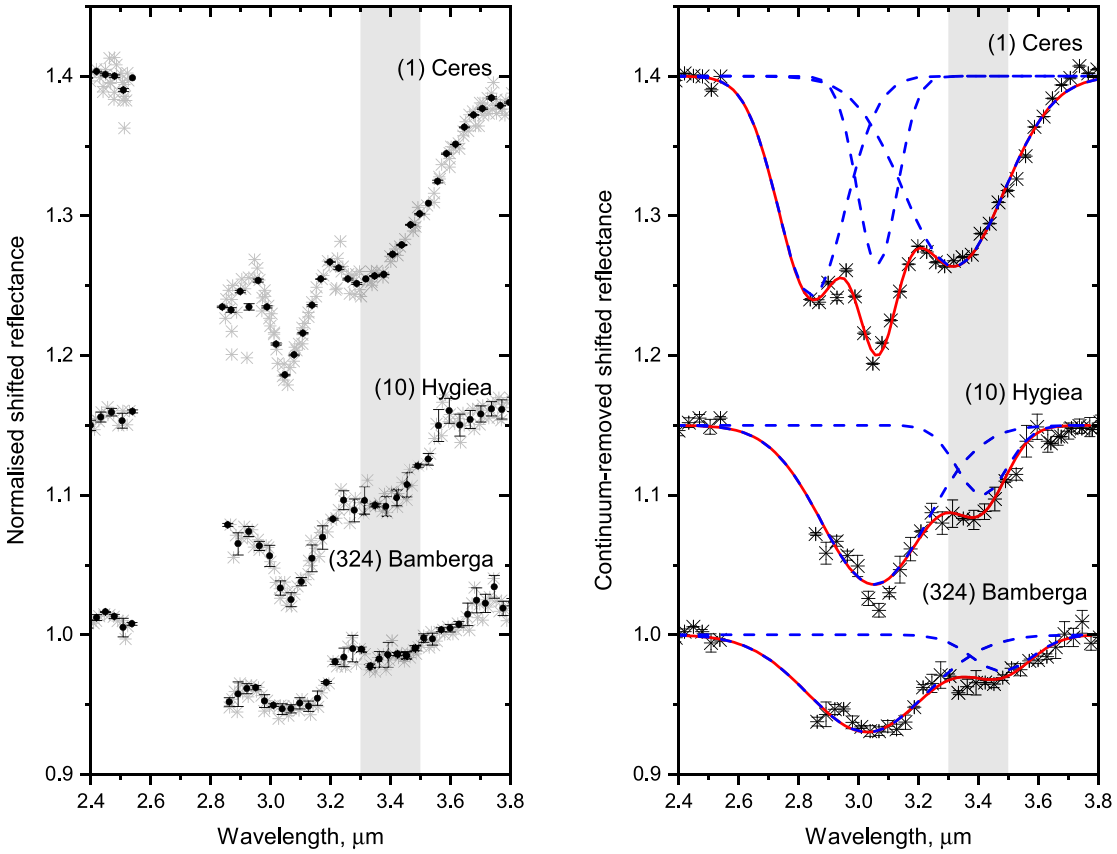

Figure 3. Ceres type spectra showing the 3.4 μm feature. The spectrum of (1) Ceres is from Rivkin et al. (2011), and the spectra of (10) Hygiea and (324) Bamberga are from Rivkin et al. (2019). The spectra are shifted for clarity. The left-hand panel shows the reflectance normalized at 2.4 μm. The original digitized spectra for which the binning was applied are shown in grey. The right-hand panel shows continuum-removed spectra together with the fit of the overall spectrum using multiple Gaussian functions (solid red line) and the individual Gaussian functions used to fit each spectrum (dashed blue line). The 3.3–3.5 μm grey area highlights the 3.4 μm absorption band. The error bars for (1) Ceres are inside the symbols.

reach beyond 3.6 μm are available in de Sanctis et al. (2018) and Merlin et al. (2021), respectively. And for (162173) Ryugu, we have the samples of the surface material that were returned to Earth Yada et al. (2021) and Pilorget et al. (2021). In particular, high-resolution near-infrared spectra were measures for samples from Chamber A that collected uppermost materials and Chamber C that collected excavated subsurface materials (Yada et al. 2021). The analysed spectra are shown in Fig. 6. Table 3 shows the calculated band parameters for the in *situ* and sample spectra.

The measured absorption band parameters for Ceres are similar to those from ground-based observations. Whereas, for Bennu and Ryugu, no ground-based spectral data are available in this region. Both Bennu and Ryugu have 'sharp'-type spectra according to Takir & Emery (2012) classification. However, the spectra of Ryugu have slightly deeper 3 and 3.4 μm absorption bands and redder spectral slope in the near-infrared region. The two spectra that correspond to samples from Chamber A and C are very similar to each other in both continuum behaviour and band parameters (Fig. 6).

4 DISCUSSION

The 3.4 μm absorption band was detected for 16 out of the 42 analysed objects. The majority of spectra with a detected 3.4 μm feature come from Takir & Emery (2012), Rivkin et al. (2019), and Usui et al. (2019), where the authors report the parameters of the 3 μm band. We found that the positions of the 3 μm band calculated in this work are in a generally good agreement with those reported in the literature. The band depth, however, cannot be directly compared due to the use of different approaches in deriving the band parameters. The presence of an absorption band around 3.4 μm was not discussed in Takir & Emery (2012) and Usui et al. (2019). Thus, the calculated parameters for the spectra reported by these authors are given here for the first time. In Rivkin et al. (2019) the authors discuss the presence of an absorption band around 3.3–3.4 μm in some of the spectra, and the parameters of the band were found using a polynomial fit over the 2.9–3.4 μm region.

It should be mentioned that nitrous oxide (N_2O) in Earth's atmosphere presents a few absorption features in the 2.8–4.2 μm range, investigated in this work. The main features are located at 2.86–2.9 μm, and 3.85–3.97 μm and a minor thin one located at 3.575 $\pm$ 0.005 μm (the bands positions are from the NIST database[3]). Fortunately, none of these features affect the continuum estimation. However, two of the three bands could affect the band depth computation, especially the 2.86–2.9 μm band, which is much stronger than the 3.575 μm band. This could hamper the accuracy of

[3]https://webbook.nist.gov/chemistry/form-ser/

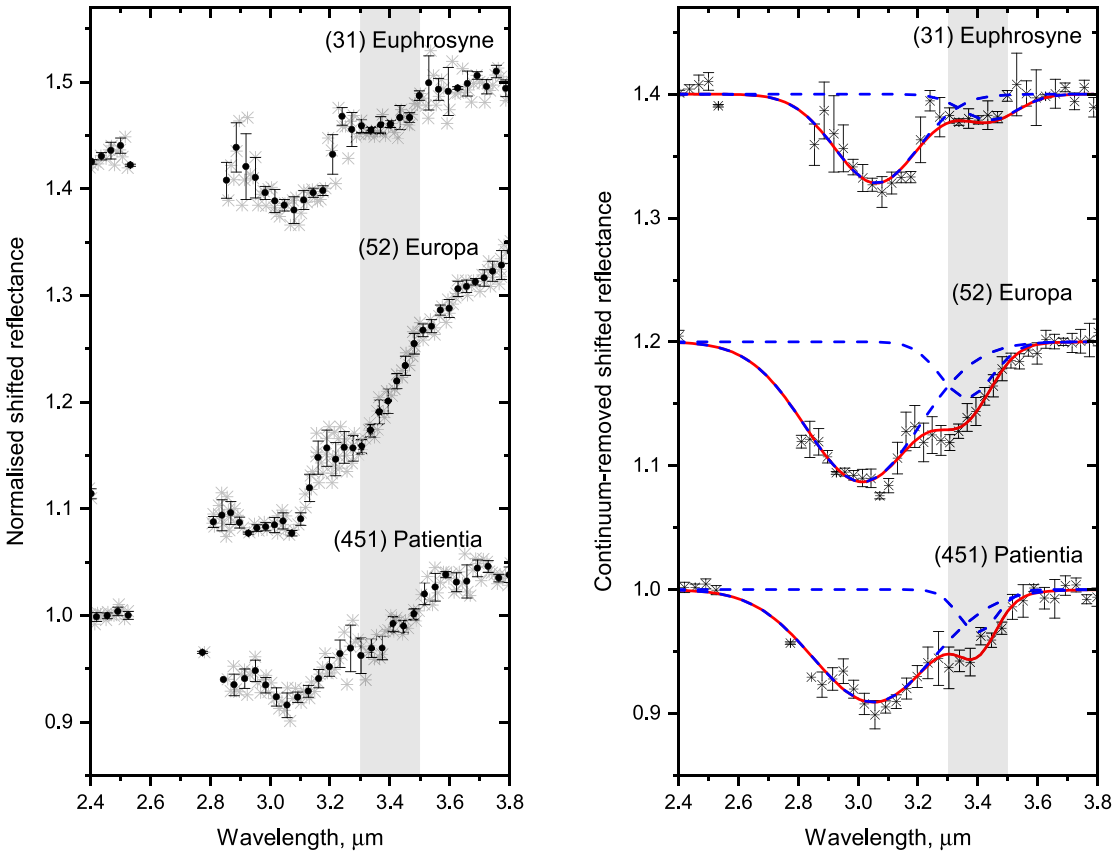

Figure 4. Europa type spectra showing the 3.4 μm feature. Spectra of (31) Euprosyne and (451) Patientia are from Rivkin et al. (2019), and the spectrum of (52) Europa is from Takir & Emery (2012). The spectra are shifted for clarity. The left-hand panel shows the reflectance normalized at 2.4 μm. The original digitized spectra for which the binning was applied are shown in grey. The right-hand panel shows continuum-removed spectra together with the fit of the overall spectrum using multiple Gaussian functions (solid red line) and the individual Gaussian functions used to fit each spectrum (dashed blue line). The 3.3–3.5 μm grey area highlights the 3.4 μm absorption band.

the whole 3 μm band depth and position estimations, while relative errors due to bad atmospheric nitrous oxide removal correction on the specific 3.4 μm band, related to C-bearing materials, are expected to be limited.

We compared surface colours and albedos for asteroids with and without a detected 3.4 μm band. Fig. 7 (left-hand panel) illustrates a U-V versus J-K colour–colour diagram. The plot suggests that asteroids with a carbon-bearing absorption feature have redder J-K colours and more neutral U-V colours. Thus, to confirm this difference, we calculated their mean colour values. For asteroids with a detected band, we found the mean colours $U - V = 1.03 \pm 0.02$ and $J - K = 0.50 \pm 0.02$, whereas for the objects with no detected band the found mean colours are $U - V = 1.09 \pm 0.02$ and $J - K = 0.43 \pm 0.03$. The reported uncertainties correspond to the standard error. From these mean colours, we can conclude that indeed there is a small difference between the colours of these two groups. Fig. 7 (right-hand panel) presents geometric albedo versus U-V colour. On this plot, we note a tendency for asteroids with a detected 3.4 μm band to have lower albedo. Again, to check this, we calculated the mean albedo value for each group. We found that for the objects with and without a detected carbon-bearing absorption feature the mean albedos are $p_V = 0.049 \pm 0.002$ and $p_V = 0.055 \pm 0.002$, respectively.

The distribution of semimajor axes and diameters for objects with and without a detected band around 3.4 μm is reported in Fig. 8. A certain difference is seen in the distributions of semimajor axes (Fig. 8, left-hand panel). Asteroids having the 3.4 μm absorption band in their spectra reside at further distances than those without the feature. This could be related to the distribution of C-type asteroids in the main belt, which are predominately located in the outer asteroid belt. According to Moroz et al. (1998), higher temperatures (i.e. smaller distances from the Sun) produce a loss of the aliphatic H-rich components. However, as it was mentioned, the 3.4 μm feature in the spectra of near-Earth asteroid Bennu was attributed to a mix of organic and carbonate materials (Simon et al. 2020), and we can expect that even more primitive asteroids that are located close to the Sun could have carbon-bearing materials on their surfaces.

The size distributions of the two groups also have some differences (Fig. 8, right-hand panel). Notably, all the asteroids in this work with sizes larger than ~300 km have a 3.4 μm absorption band. This could be explained by a bias, as larger objects in the analysed data set tend to have spectra with higher S/N ratio (as can be seen in Fig. 1). Additionally, we found no correlation between the size of an object and the depth of the 3.4 μm band.

Asteroids with a detected 3.4 μm band have a variety of orbital and physical parameters. And even though our data set is rather small, we also searched for possible correlations between the detected

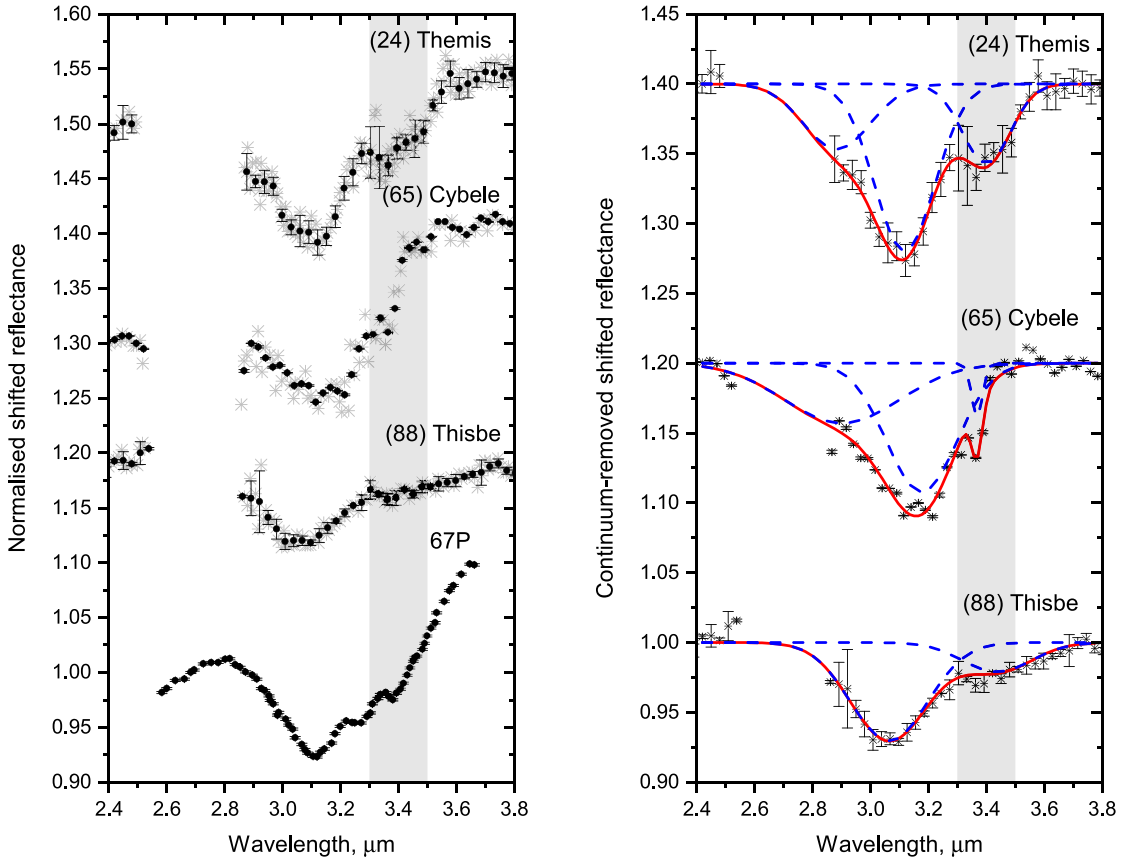

Figure 5. 'Rounded' type spectra showing the 3.4 μm feature. The spectrum of (24) Themis is from Rivkin & Emery (2010), (65) Cybele is from Licandro et al. (2011), (88) Thisbe is from Rivkin et al. (2019), and the spectrum of the comet 67P is from Raponi et al. (2020). The spectra are shifted for clarity. The left-hand panel shows the reflectance normalized at 2.4 μm. The original digitized spectra for which the binning was applied are shown in grey. The right-hand panel shows continuum-removed spectra together with the fit of the overall spectrum using multiple Gaussian functions (solid red line) and the individual Gaussian functions used to fit each spectrum (dashed blue line). The 3.3–3.5 μm grey area highlights the 3.4 μm absorption band. The error bars for (65) Cybele and comet 67P are inside the symbols.

absorption around 3.4 μm and orbital parameters. However, we did not find any clear correlation between the calculated band parameters (band depth and position) and the orbital elements (e, i, a, q, Q).

To study the relationship between carbon-bearing and OH-bearing compounds, we compared the depth of the 3.4 μm band with that of the 3 μm band. For the objects with multiple spectra available, we observe a difference in band parameters that could be associated with surface heterogeneity. Fig. 9 shows 3 μm band depth versus 3.4 μm band depth for all the spectra in Tables 2 and 3. When we considered individual groups, we found a strong correlation for the Ceres-like, Europa-like, and 'rounded' types, with Pearson's correlation coefficient r = 0.98 for these three groups combined. However, the number of data points in each group is rather small for a conclusive result. The 'sharp'-group objects seem to have a somewhat different dependence. However, the band parameters were measured only for three 'sharp'-type spectra, so we do not report the correlation coefficient for this group. Previous works have shown that the depth of the 3.4 μm band in the spectra of IOM and carbonaceous meteorites is correlated with the H/C ratio, bulk C, and organic-bound H (Kaplan, Milliken & Alexander 2018; Kaplan et al. 2019), whereas the depth of the 3 μm band is related to the H/OH/H_2O abundance (Beck et al. 2018; Garenne et al. 2016). Thus, the correlation between the 3 and 3.4 μm bands for the studied asteroids may suggest a relation between the bulk hydrogen content and the organic hydrogen content.

4.1 Carbon-bearing materials on space mission targets

Comet 67P/Churyumov-Gerasimenko shows the ubiquitous presence of organic matter with a bulk composition similar to the IOM extracted from primitive chondrites (Capaccioni et al. 2015; Quirico et al. 2016; Raponi et al. 2020). The comet dust appears to have higher C/Si and H/C ratios compared to carbonaceous chondrites IOM (Fray et al. 2016; Bardyn et al. 2017). Recent recalibrations of the VIRTIS spectrometer permitted the identification of several sub-features within the broad absorption band between 2.8 and 3.6 μm (Raponi et al. 2020), the stronger being centred at 3.1, 3.3, 3.38, 3.42, and 3.47 μm. The absorption bands identified at 3.38 and 3.42 μm have been assigned to asymmetric C-H stretching modes of the methyl (CH_3) and methylene (CH_2) aliphatic groups, respectively, while the one at 3.47 μm is attributed to the symmetric modes of CH_3 and CH_2 groups (Raponi et al. 2020). The two most intense absorption bands at 3.1 and 3.3 μm in the average spectrum of comet 67P are attributed to N-H vibrations modes in ammonium salts, although a contribution of PAHs at 3.3 μm cannot be excluded (Quirico et al. 2016; Poch et al. 2020; Raponi et al. 2020). The

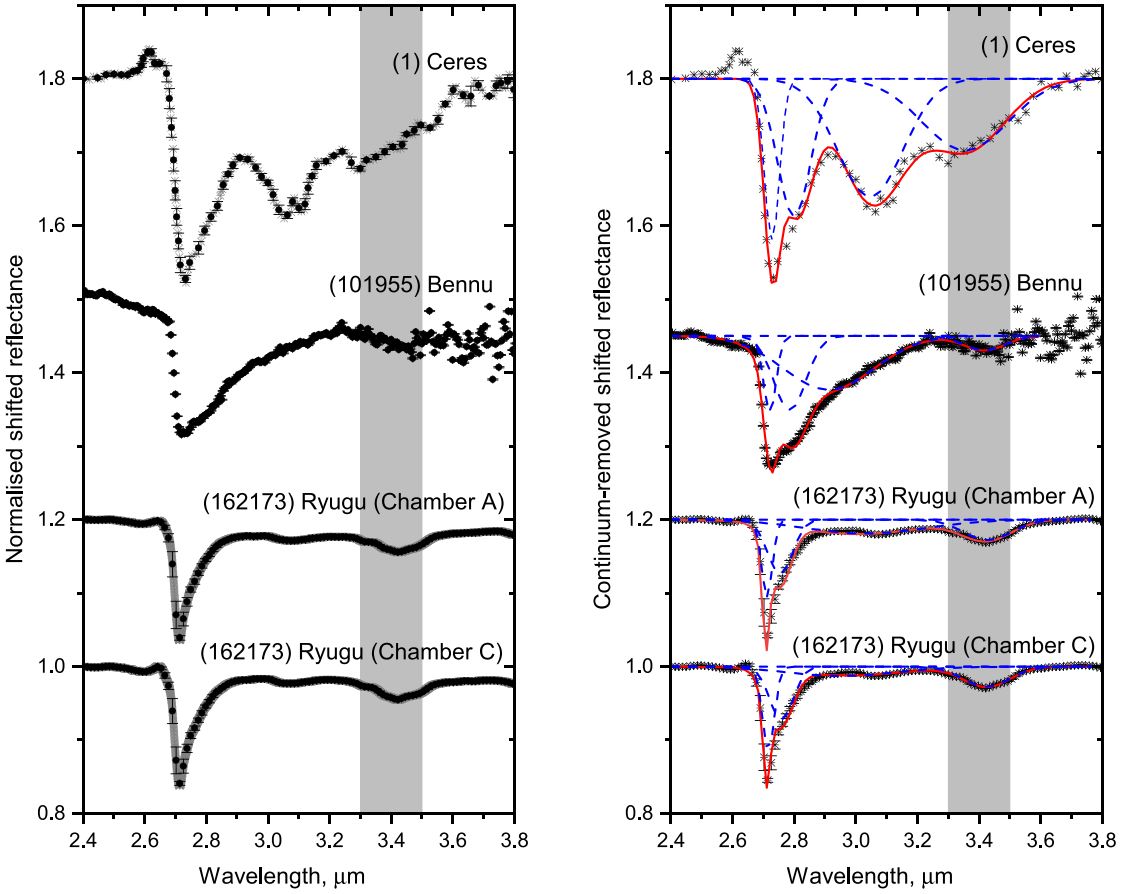

Figure 6. Infrared spectra of space mission targets showing the 3.4 μm feature. The spectrum of (1) Ceres is from de Sanctis et al. (2018), and the spectra of (101955) Bennu and (162173) Ryugu are from Merlin et al. (2021) and Yada et al. (2021), respectively. The spectra are shifted for clarity. The left-hand panel shows the reflectance normalized at 2.4 μm. The original digitized spectrum of (1) Ceres is shown in grey. The right-hand panel shows continuum-removed spectra together with the fit of the overall spectrum using multiple Gaussian functions (solid red line) and the individual Gaussian functions used to fit each spectrum (dashed blue line). The 3.3–3.5 μm grey area highlights the 3.4 μm absorption band.

Table 3. Characteristics of the 3 and 3.4 μm bands for the low-albedo asteroids visited by space missions.

Object	3 μm band centre, μm	3.4 μm band centre, μm	3 μm band depth, per cent	3.4 μm band depth, per cent	3 μm type∗	Spectrum reference
(1) Ceres	2.726 ± 0.002	3.346 ± 0.008	21.81 ± 0.70	9.86 ± 0.09	Ceres-type	de Sanctis et al. (2018)
(101955) Bennu	2.753 ± 0.001	3.409 ± 0.001	12.81 ± 0.03	1.87 ± 0.02	Sharp	Merlin et al. (2021)
(162173) Ryugu (Chamber A)	2.759 ± 0.004	3.426 ± 0.001	14.31 ± 0.56	2.78 ± 0.02	Sharp	Yada et al. (2021)
(162173) Ryugu (Chamber C)	2.760 ± 0.004	3.424 ± 0.001	14.63 ± 0.47	2.75 ± 0.02	Sharp	Yada et al. (2021)

∗Following the classification by Takir & Emery (2012).

aliphatic features detected on comet 67P are compatible both with the aliphatic ISM ones and with those of primitive IOM chondrites (Raponi et al. 2020).

Using a high-resolution spectrometer on-board, the Dawn spacecraft De Sanctis et al. (2019) made detailed analyses of the organic-rich areas on the surface of Ceres. De Sanctis et al. (2019) identified hundreds of meters-size areas that seem to be particularly rich in aliphatic organics, and the authors suggest that the aliphatic organic on Ceres is an endogenous product. Vinogradoff et al. (2021) found that the organic-rich spectrum of Ceres is best reproduced by a mixture containing about 20 wt. per cent of carbon (a third being aliphatic carbons). In Fig. 10, we present the spectra of Ceres, taken from De Sanctis et al. (2019), relative to two different areas rich in carbonates and organics. Additionally, we plot in Fig. 10 the laboratory spectra from the RELAB database of the dark calcite (CB-EAC-013-B) sample and of the CI1 meteorite Alais (MTKTH-264), also showing organic absorption bands. We can see a difference both in shape and depth of the 3.4 μm band in the two spectra of Ceres. Moreover, a 4 μm band that corresponds to carbonates is more pronounced in the spectrum associated with a carbonate-rich area of Ceres. The band analysis done on the high-quality spectra obtained by Dawn mission confirm the measured band depth obtained by telescopic observations (see Tables 2 and 3).

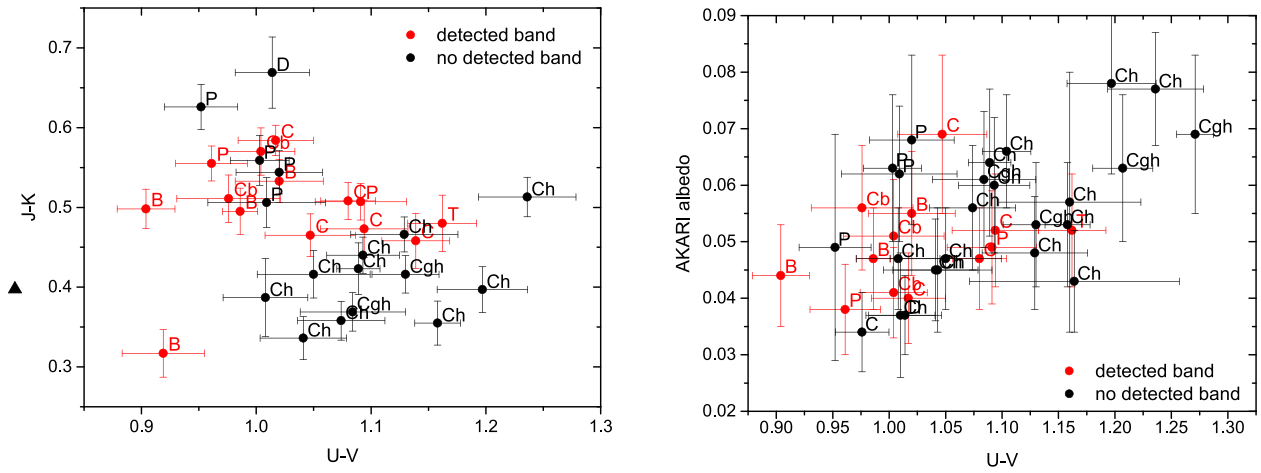

Figure 7. Left-hand panel: U-V versus J-K colours for asteroids in our data set. There is a tendency for asteroids with the 3.4 μm band to have redder J-K colours and more neutral U-V colours. Right-hand panel: U-V colour versus albedo value taken from the AKARI survey. The plot shows that objects with the 3.4 μm band tend to have lower albedo. The largest asteroids in the data set (1) Ceres and (2) Pallas are not shown in this plot.

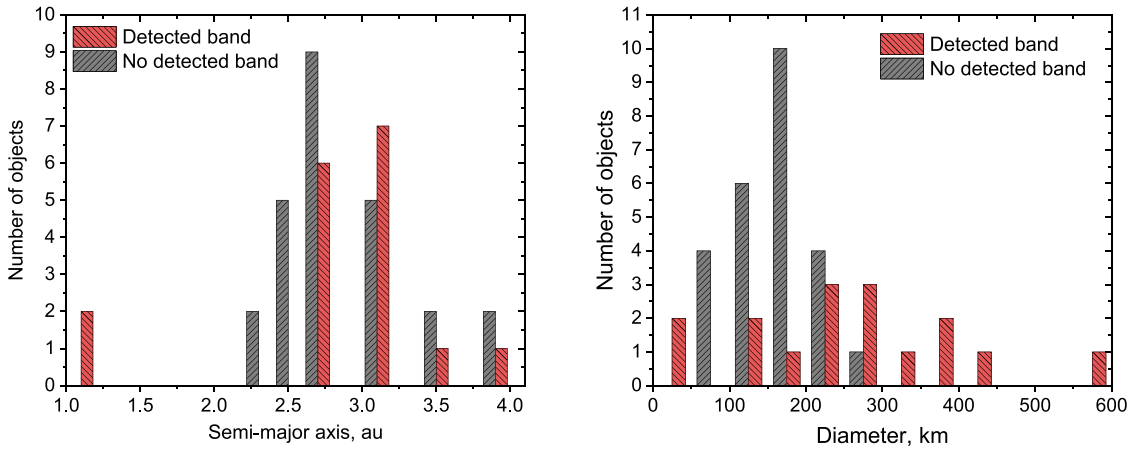

Figure 8. Comparison of asteroids in our data set (N = 42) that show evidence of an absorption band at 3.4 μm (N = 16) with those that do not (N = 26).

Kaplan et al. (2020) and Simon et al. (2020) studied the Nightingale crater region on the surface of Bennu from the OSIRIS-REx mission visible and near-infrared spectra. These authors were able to distinguish organic and carbonate features by comparing them to the laboratory spectra of carbonates and organics. They found that carbonates have two minima near 3.4 μm, whereas aliphatic organics have one minimum at 3.42 μm. Kaplan et al. (2020) showed that the strongest organic absorption features they identified are associated with redder and darker material. Moreover, Ferrone et al. (2021) distinguished organic and carbonate absorption features in higher-spatial-resolution spectra of Bennu's surface by using the Kolmogorov–Smirnov test. They found that organics are either widespread across Bennu's surface or that the spatial resolution of the analysed spectra prohibits them from detecting correlations between organic features and Bennu's surface spectral properties.

The laboratory analysis of the material collected on Ryugu by Hayabusa2 showed that it is a representative of the asteroid's surface. The returned samples have dark near-infrared spectra with absorption features at 2.7 and 3.4 μm. The spectra are most similar to that of CI chondrites but are darker and more porous (Yada et al. 2021). A clear absorption band appears at 3.4 μm at global scale (Yada et al. 2021); while distinctive signatures (carbonates as well as NH-rich compounds) are detected when analysed at submillimetric scale (Pilorget et al. 2021).

5 SUMMARY

The study of pristine organic materials is pivotal for understanding the origin of life on Earth and unraveling the processes that were occurring at the early stages of Solar System formation (Brack 1993; Kwok 2009; Altwegg et al. 2015).

This work presents the first homogeneous analysis of spectroscopic features due to carbon-bearing compounds in spectra of low-albedo asteroids using the entire available data set with sufficient data quality.

Following the classification proposed by Takir & Emery (2012) we divided the asteroids showing a 3.4 μm feature into 4 groups. For Ceres-like, Europa-like, and 'rounded' groups of spectra we found a

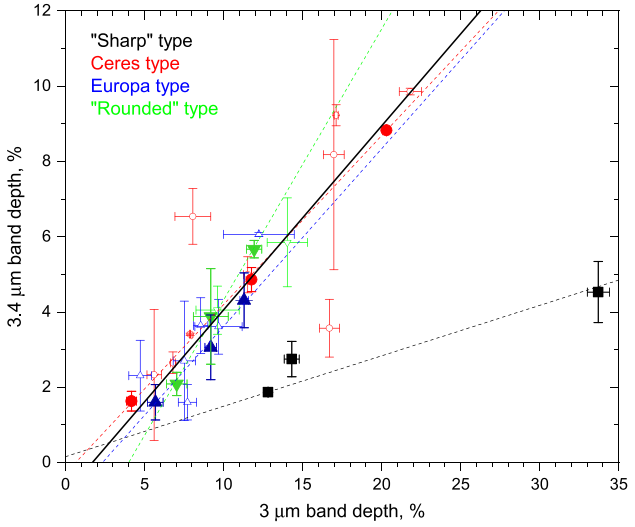

Figure 9. 3 μm band depth versus 3.4 μm band depth. The different colours correspond to the four types of 3 μm band shape from Takir & Emery (2012). Filled symbols correspond to the best/only spectra for each object in the data set. Empty symbols correspond to the band parameters with higher uncertainties when multiple spectra are available. The weighted linear fit for the Ceres-like, Europa-like, and 'rounded' types is shown separately with dashed lines, and the fit for all three types is shown with a solid black line.

strong correlation (r = 0.98) between the depth of the 3.4 μm band, which could be related to carbon-bearing compounds, and the depth of the 3 μm band, associated with OH-bearing materials and water ice.

The objects with a detected 3.4 μm band in our data set have lower albedo, redder J-K colours, and more neutral U-V colours. Spectral types are not distributed evenly among objects with and without the 3.4 μm band: the majority of spectra not showing the 3.4 μm band belong to the Ch or Chg classes but are affected by their low SNR.

The 3.4 μm band was found for all asteroids in the data set that are larger than ∼300 km, which is most probably related to a correlation of S/N ratio and diameter. Also, among the analysed asteroids, the objects with a detected 3.4 μm band tend to be located at larger distances from the Sun than those without a detected 3.4 μm band.

Space telescopes are needed to avoid the drastic telluric absorption in the 3–4 μm wavelength range. Additionally, the search for possible absorption bands in the spectra of smaller size asteroids requires the use of big ground-based telescopes. In this regard, the *James Webb Space Telescope* and a new generation of telescopes such as the *Thirty Meter Telescope* in Hawaii could help us to conduct a much more thorough investigation of primitive Solar System bodies and advance our knowledge about the past of our Solar System.

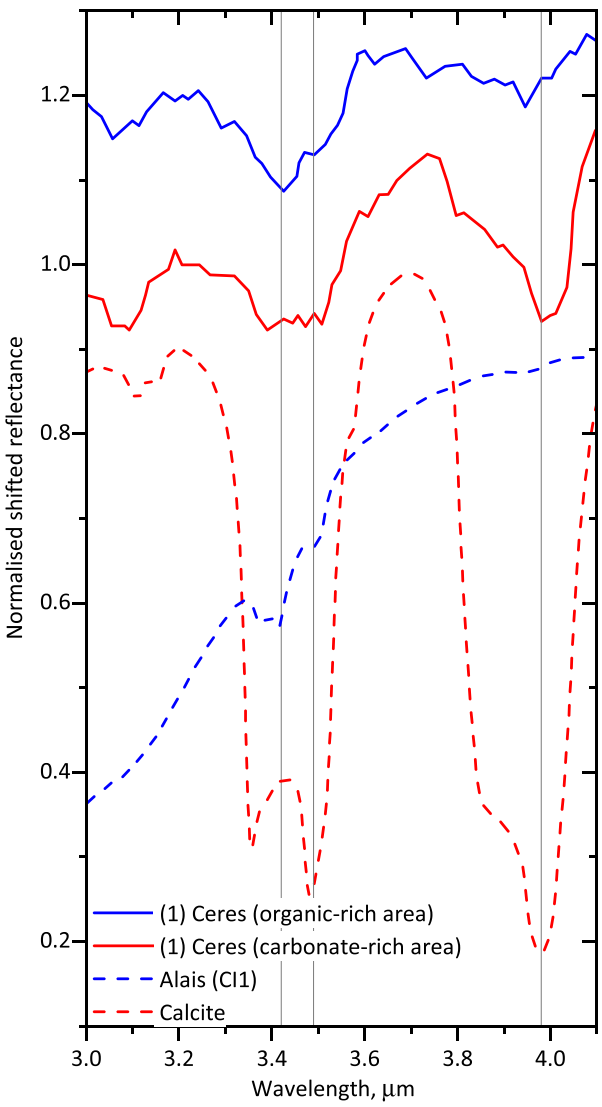

Figure 10. Spectra covering the 3 μm region of organic-rich (blue solid line) and carbonate-rich (red solid line) regions on the surface of (1) Ceres De Sanctis et al. (2019). We also show the laboratory spectra of dark calcite (dashed red line) and CI1 meteorite Alais (dashed blue line) taken from the RELAB database. Vertical lines show the position of the absorption bands associated with organics and carbonates. The spectra were normalized at 3.2 μm and shifted for clarity.

ACKNOWLEDGEMENTS

We acknowledge funding from the European Union's Horizon 2020 research and innovation programme under grant agreement no. 870403. We thank the reviewer Driss Takir for his comments which improved the quality of the paper.

DATA AVAILABILITY

The data underlying this article were partially derived from the PDS Small Bodies Node (https://pds.nasa.gov/ds-view/pds/viewProfile.jsp?dsid=EAR-A-3-RDR-THREEMICRON-V1.1) and AKARI (https://www.ir.isas.jaxa.jp/AKARI/Archive/) databases. The data can also be shared on reasonable request to the corresponding author.

REFERENCES

Alexander C. M. O. D., Fogel M., Yabuta H., Cody G. D., 2007, Geochim. Cosmochim. Acta, 71, 4380
Alexander C. M. O., Cody G. D., Kebukawa Y., Bowden R., Fogel M. L., Kilcoyne A. L. D., Nittler L. R., Herd C. D. K., 2014, Meteorit. Planet. Sci., 49, 503
Alexander C. M. O. D., Cody G. D., De Gregorio B. T., Nittler L. R., Stroud R. M., 2017, Chem. der Erde Geochem., 77, 227
Alí-Lagoa V., Müller T. G., Usui F., Hasegawa S., 2018, A&A, 612, A85
Altwegg K. et al., 2015, Science, 347, 1261952
Bardyn A. et al., 2017, MNRAS, 469, S712
Beck P., Maturilli A., Garenne A., Vernazza P., Helbert J., Quirico E., Schmitt B., 2018, Icarus, 313, 124
Bell J. F., 1989, Icarus, 78, 426
Botta O., Bada J. L., 2002, Surv. Geophys., 23, 411
Brack A., 1993, Orig. Life Evol. Biosph., 23, 3
Brad Dalton J., Cruikshank D. P., Clark R. N., 2012, Icarus, 220, 752
Brown M. E., 2016, AJ, 152, 159
Brown M. E., Rhoden A. R., 2014, ApJ, 793, L44
Busemann H., Young A. F., O'D. Alexander C. M., Hoppe P., Mukhopadhyay S., Nittler L. R., 2006, Science, 312, 727
Campins H. et al., 2010, Nature, 464, 1320
Capaccioni F. et al., 2015, Science, 347, aaa0628
Cody G. D., Alexander C. M. O. D., 2005, Geochim. Cosmochim. Acta, 69, 1085
Cruikshank D. P., Brown R. H., 1987, Science, 238, 183
Cruikshank D. P., Geballe T. R., Owen T. C., Dalle Ore C. M., Roush T. L., Brown R. H., Lewis J. H., 2002, Icarus, 156, 434
Cruikshank D. P., Dalle Ore C. M., Clark R. N., Pendleton Y. J., 2014, Icarus, 233, 306
de Sanctis M. C. et al., 2018, Meteorit. Planet. Sci., 53, 1844
De Sanctis M. C. et al., 2017, Science, 355, 719
De Sanctis M. C. et al., 2019, MNRAS, 482, 2407
DeMeo F. E., Binzel R. P., Slivan S. M., Bus S. J., 2009, Icarus, 202, 160
Ehrenfreund P., Robert F., D'Hendecourt L., Behar F., 1991, A&A, 252, 712
Feierberg M. A., Lebofsky L. A., Tholen D. J., 1985, Icarus, 63, 183
Ferrone S. M. et al., 2021, Icarus, 368, 114579
Fomenkova M. N., Chang S., Mukhin L. M., 1994, Geochim. Cosmochim. Acta, 58, 4503
Fray N. et al., 2016, Nature, 538, 72
Gaffey M. J., Burbine T. H., Binzel R. P., 1993, Meteoritics, 28, 161
Garenne A. et al., 2016, Icarus, 264, 172
Hargrove K. D., Kelley M. S., Campins H., Licandro J., Emery J., 2012, Icarus, 221, 453
Hayes J. M., 1967, Geochim. Cosmochim. Acta, 31, 1395
Jones T. D., Lebofsky L. A., Lewis J. S., Marley M. S., 1990, Icarus, 88, 172
Kaplan H. H., Milliken R. E., Alexander C. M. O., 2018, Geophys. Res. Lett., 45, 5274
Kaplan H. H., Milliken R. E., Alexander C. M. O., Herd C. D. K., 2019, Meteorit. Planet. Sci., 54, 1051
Kaplan H. H. et al., 2020, Science, 370, eabc3557
Kebukawa Y., Nakashima S., Zolensky M. E., 2010a, Meteorit. Planet. Sci., 45, 99
Kebukawa Y., Nakashima S., Ishikawa M., Aizawa K., Inoue T., Nakamura-Messenger K., Zolensky M. E., 2010b, Meteorit. Planet. Sci., 45, 394
Keller L. P., Messenger S., Flynn G. J., Clemett S., Wirick S., Jacobsen C., 2004, Geochim. Cosmochim. Acta, 68, 2577
Kwok S., 2009, Ap&SS, 319, 5
Lauretta D. S. et al., 2019, Nature, 568, 55
Lebofsky L. A., Feierberg M. A., Tokunaga A. T., Larson H. P., Johnson J. R., 1981, Icarus, 48, 453
Licandro J., Campins H., Kelley M., Hargrove K., Pinilla-Alonso N., Cruikshank D., Rivkin A. S., Emery J., 2011, A&A, 525, A34
Mennella V., 2010, ApJ, 718, 867
Merlin F. et al., 2021, A&A, 688, A88
Moroz L. V., Arnold G., Korochantsev A. V., Wäsch R., 1998, Icarus, 134, 253
Müller T. G. et al., 2017, A&A, 599, A103
Nakamura-Messenger K., Messenger S., Keller L. P., Clemett S. J., Zolensky M. E., 2006, Science, 314, 1439
Nuevo M., Sandford S. A., Flynn G. J., Wirick S., 2014, Meteorit. Planet. Sci., 49, 2017
Orthous-Daunay F. R., Quirico E., Beck P., Brissaud O., Dartois E., Pino T., Schmitt B., 2013, Icarus, 223, 534
Park R. S. et al., 2016, Nature, 537, 515
Pieters C. M., McFadden L. A., 1994, Annu. Rev. Earth Planet. Sci., 22, 457
Pilorget C. et al., 2021, Nature Astron., 6, 221
Pizzarello S., Cooper G. W., Flynn G. J., 2006, in Lauretta D. S., McSween H. Y., Jr, eds, Meteorites and the Early Solar System II. University of Arizona Press, Tucson, p. 625
Poch O. et al., 2020, Science, 367, aaw7462
Praet A. et al., 2021, Icarus, 363, 114427
Quirico E. et al., 2016, Icarus, 272, 32
Raponi A. et al., 2020, Nature Astron., 4, 500
Rivkin A. S., Emery J. P., 2010, Nature, 464, 1322
Rivkin A. S., Volquardsen E. L., Clark B. E., 2006, Icarus, 185, 563
Rivkin A. S., Li J.-Y., Milliken R. E., Lim L. F., Lovell A. J., Schmidt B. E., McFadden L. A., Cohen B. A., 2011, Space Sci. Rev., 163, 95
Rivkin A. S. et al., 2013, Icarus, 223, 493
Rivkin A. S., Thomas C. A., Howell E. S., Emery J. P., 2015, AJ, 150, 198
Rivkin A. S., Howell E. S., Emery J. P., 2019, J. Geophys. Res. (Planets), 124, 1393
Robert F., Epstein S., 1982, Geochim. Cosmochim. Acta, 46, 81
Rohatgi A., 2021, Webplotdigitizer: Version 4.5, [Last accessed on January 4, 2021] https://automeris.io/WebPlotDigitizer
Schmitt-Kopplin P. et al., 2010, Proc. Natl. Acad. Sci., 107, 2763
Simon A. A. et al., 2020, Science, 370, eabc3522
Sykes M. V., Cutri R. M., Skrutskie M. F., Fowler J. W., Tholen D. J., Painter P. E., Nelson B., Kirkpatrick D. J., 2010, NASA Planetary Data System, pp EAR–A–I0054/I0055–5–2MASS–V2.0
Takir D., Emery J. P., 2012, Icarus, 219, 641
Takir D., Emery J. P., McSween H. Y., Hibbitts C. A., Clark R. N., Pearson N., Wang A., 2013, Meteorit. Planet. Sci., 48, 1618
Takir D., Stockstill-Cahill K. R., Hibbitts C. A., Nakauchi Y., 2019, Icarus, 333, 243
Tatsumi E. et al., 2020, A&A, 639, A83
Tedesco E. F., 2005, NASA Planetary Data System, pp EAR–A–5–DDR–UBV–MEAN–VALUES–V1.2
Tholen D. J., 1984, PhD thesis, University of Arizona
Usui F., Hasegawa S., Ootsubo T., Onaka T., 2019, PASJ, 71, 1
Vinogradoff V. et al., 2021, Minerals, 11, 719
Watanabe S.-I., Tsuda Y., Yoshikawa M., Tanaka S., Saiki T., Nakazawa S., 2017, Space Sci. Rev., 208, 3
Yada T. et al., 2021, Nature Astron., 6, 214

APPENDIX A: LIST OF ALL LOW-ALBEDO OBJECTS IN THE DATA SET

continued

	Object	SNR	Reference
1	(1) Ceres	173	Rivkin et al. (2011)
2	(2)Pallas	52	Usui et al. (2019)
3	(10) Hygiea	138	Rivkin et al. (2019)
4	(13) Egeria	63	Usui et al. (2019)
5	(19) Fortuna	32	Usui et al. (2019)
6	(24) Themis	50	Rivkin & Emery (2010)
7	(31) Euphrosyne	122	Rivkin et al. (2019)
8	(34) Circe	18	Takir & Emery (2012)
9	(36) Atalante	17	Takir & Emery (2012)
10	(38) Leda	12	Rivkin et al. (2015)
11	(41) Daphne	64	Rivkin et al. (2015)
12	(46) Hestia	19	Usui et al. (2019)
13	(48) Doris	35	Takir & Emery (2012)
14	(49) Pales	23	Usui et al. (2019)
15	(50) Virginia	23	Usui et al. (2019)
16	(51) Nemausa	215	Rivkin et al. (2015)
17	(52) Europa	124	Takir & Emery (2012)
18	(54) Alexandra	35	Takir & Emery (2012)
19	(56) Melete	22	Usui et al. (2019)
20	(65) Cybele	216	Licandro et al. (2011)
21	(66) Maja	18	Rivkin et al. (2015)
22	(70) Panopaea	152	Rivkin et al. (2015)
23	(74) Galatea	5	Feierberg et al. (1985)
24	(76) Freia	10	Takir & Emery (2012)
25	(78) Diana	49	Rivkin et al. (2015)
26	(81) Terpsichore	19	Usui et al. (2019)
27	(87) Sylvia	18	Usui et al. (2019)
28	(88) Thisbe	220	Rivkin et al. (2019)
29	(90) Antiope	9	Lebofsky et al. (1981)
30	(91) Aegina	24	Takir & Emery (2012)
31	(94) Aurora	17	Usui et al. (2019)
32	(104) Klymene	8	Takir & Emery (2012)
33	(105) Artemis	37	Rivkin et al. (2015)
34	(106) Dione	25	Usui et al. (2019)
35	(107) Camilla	23	Takir & Emery (2012)
36	(109) Felicitas	33	Rivkin et al. (2015)
37	(120) Lachesis	11	Takir & Emery (2012)
38	(121) Hermione	25	Usui et al. (2019)
39	(127) Johanna	13	Usui et al. (2019)
40	(128) Nemesis	17	Usui et al. (2019)
41	(130) Elektra	25	Takir & Emery (2012)
42	(139) Juewa	5	Feierberg et al. (1985)
43	(140) Siwa	25	Takir & Emery (2012)
44	(144) Vibilia	33	Rivkin et al. (2015)
45	(145) Adeona	18	Usui et al. (2019)
46	(153) Hilda	10	Takir & Emery (2012)
47	(156) Xanthippe	13	Rivkin et al. (2015)
48	(159) Aemilia	9	Rivkin et al. (2015)
49	(163) Erigone	18	Rivkin et al. (2015)
50	(168) Sibylla	13	Rivkin et al. (2015)
51	(173) Ino	16	Usui et al. (2019)
52	(176) Iduna	10	Rivkin et al. (2015)
53	(185) Eunike	18	Usui et al. (2019)
54	(187) Lamberta	12	Takir & Emery (2012)
55	(190) Ismene	24	Takir & Emery (2012)
56	(200) Dynamene	19	Rivkin et al. (2015)
57	(207) Hedda	17	Rivkin et al. (2015)
58	(211) Isolda	15	Rivkin et al. (2015)
59	(247) Eukrate	5	Feierberg et al. (1985)
60	(308) Polyxo	47	Takir & Emery (2012)
61	(324) Bamberga	150	Rivkin et al. (2019)
62	(334) Chicago	22	Takir & Emery (2012)
63	(335) Roberta	18	Rivkin et al. (2013)
64	(336) Lacadiera	8	Usui et al. (2019)
65	(344) Desiderata	5	Feierberg et al. (1985)
66	(345) Tercidina	13	Rivkin et al. (2015)
67	(361) Bononia	111	Takir & Emery (2012)
68	(386) Siegena	5	Feierberg et al. (1985)
69	(401) Ottilia	7	Takir & Emery (2012)
70	(404) Arsinoe	28	Rivkin et al. (2015)
71	(405) Thia	13	Rivkin et al. (2015)
72	(407) Arachne	32	Rivkin et al. (2015)
73	(410) Chloris	5	Feierberg et al. (1985)
74	(419) Aurelia	16	Usui et al. (2019)
75	(423) Diotima	23	Usui et al. (2019)
76	(451) Patientia	98	Rivkin et al. (2019)
77	(476) Hedwig	29	Usui et al. (2019)
78	(511) Davida	45	Takir & Emery (2012)
79	(554) Peraga	17	Rivkin et al. (2015)
80	(576) Emanuela	19	Rivkin et al. (2015)
81	(602) Marianna	13	Rivkin et al. (2015)
82	(654) Zelinda	15	Rivkin et al. (2015)
83	(694) Ekard	13	Rivkin et al. (2015)
84	(704) Interamnia	100	Rivkin et al. (2019)
85	(754) Malabar	15	Rivkin et al. (2015)
86	(773) Irmintraud	9	Usui et al. (2019)
87	(776) Berbericia	9	Rivkin et al. (2015)
88	(790) Pretoria	13	Takir & Emery (2012)
89	(791) Ani	17	Rivkin et al. (2015)
90	(1467) Mashona	7	Rivkin et al. (2015)
91	(101955) Bennu	85	Merlin et al. (2021)
92	(175706) 1996 FG3	18	Rivkin et al. (2013)

This paper has been typeset from a TEX/LATEX file prepared by the author.